

Capillary-bridge Forces Between Solid Particles: Insights from Lattice Boltzmann Simulations

Lei Yang and Marcello Sega

*Helmholtz Institute Erlangen-Nürnberg for Renewable Energy (IEK-11),
Forschungszentrum Jülich, Fürther Straße 248, 90429 Nürnberg, Germany*

Jens Harting

*Helmholtz Institute Erlangen-Nürnberg for Renewable Energy (IEK-11),
Forschungszentrum Jülich, Fürther Straße 248, 90429 Nürnberg, Germany and
Department of Chemical and Biological Engineering and Department of Physics,
Friedrich-Alexander-Universität Erlangen-Nürnberg,
Fürther Straße 248, 90429 Nürnberg, Germany*

Liquid capillary-bridge formation between solid particles has a critical influence on the rheological properties of granular materials and, in particular, on the efficiency of fluidized bed reactors. The available analytical and semi-analytical methods have inherent limitations, and often do not cover important aspects, like the presence of non-axisymmetric bridges. Here, we conduct numerical simulations of the capillary bridge formation between equally and unequally-sized solid particles using the lattice Boltzmann method, and provide an assessment of the accuracy of different families of analytical models. We find that some of the models taken into account are shown to perform better than others. However, all of them fail to predict the capillary force for contact angles larger than $\pi/2$, where a repulsive capillary force attempts to push the solid particle outwards to minimize the surface energy, especially at a small separation distance. We then apply the most suitable model to study the impact of capillary interactions on particle clustering using a coupled lattice Boltzmann and Discrete Element method.

I. INTRODUCTION

In many industrial processes such as wet granulation, coating, or drying, powders can contain a small amount of liquid. In these powders, the appearance of liquid capillary bridges between the grains generates adhesion forces at the micro-scale that can modify dramatically the granular medium's mechanical properties at the macro-scale [1]. One of the signatures of capillary bridges is the formation of agglomerates. Next to many other applications, this is for example important in the combustion of biomasses. The ash composition of biogenic fuels like energy crops or agricultural residues contains always a high amount of silicon and potassium, which are prone to melt at the operating temperatures of fluidized beds [2]. The molten ash then forms liquid bridges between particles and causes agglomeration. The growth of agglomerates, if not counteracted properly, can cause the defluidization of the bed. In this sense, understanding the interaction between solid particles as mediated by the liquid bridges is critical to reduce the limiting factors of fluidized bed reactors and to improve their performance.

In the literature one can find a considerable amount of research focusing on analytical expressions that estimate the capillary forces induced by

the bridges [3–8]. Most of these works make use of either an energetic route (i.e., via the derivative of the total interface energy) or, equivalently [9], approximate solutions of the Young-Laplace equation. Typically, once the meniscus geometry is known, the capillary force can be obtained by multiplying the cross-sectional area by the Laplace pressure and adding the surface tension of the liquid. The two main approximations employed to describe the meniscus shape are the toroidal [10, 11] and the Derjaguin [12] approximations. Several other approximate solutions of the Young-Laplace equation based on these two have been reported in literature [5, 6, 13].

Many of these approximations assume the bridge connecting two identical spherical particles. In reality, particles are often polydisperse in size, and some authors proposed theoretical models for the prediction of the capillary force for unequally-sized spheres [5, 14–16]. In addition, most studies found in literature focus on capillary bridges with small, typically less than 10%, liquid-to-solid volume ratios (e.g., [3, 5, 6, 17, 18]), whereas only few studies focus on larger volumes [15, 19, 20]. Interestingly, with a large enough liquid volume, the solution that minimizes the surface energy is not anymore axisymmetric [21], as it was also shown numerically and experimentally [19]. Moreover, when increasing the

separation distance, it is possible to observe a transition from a convex to a concave profile [20].

Numerical methods to tackle the problem of the liquid capillary bridge were devised already in the early 1970s by Erle and coworkers, obtaining a satisfactory agreement at large separation distances [22]. Generally, for static solutions, one can numerically minimize the interfacial free energy using a number of freely available tools [23]. If the dynamics of the bridge formation does play a role, CFD methods such as the volume-of-fluid (VOF) and level set methods are common choices [24, 25]. They solve the macroscopic Navier-Stokes equations by tracking or capturing the interface. An alternative approach is the lattice Boltzmann method (LBM), which became popular due to its straightforward implementation, its inherent parallelization and a wide selection of multiphase models being available [26, 27]. We would like to emphasize that the LBM can be used to model dynamic problems that are beyond of the scope of other methods based just on the minimization of surface energy as, for example, implemented in Surface Evolver [28]. In the LBM, hydrodynamics is being described at the Navier-Stokes level in the nearly incompressible limit. The dynamics of the solid particles can be simulated by solving Newton's equations of motion for the translational and rotational degrees of freedom, and coupled to the single or multicomponent fluid using various approaches[29–31]. In comparison with conventional CFD methods, the LBM is limited to low Mach numbers. Also, at high Knudsen numbers, more work is needed to improve the accuracy of the method while maintaining computational efficiency. However, these limitations have no influence on the current study of capillary bridges.

In this work, we use the multicomponent interparticle potential model by Shan and Chen [32] coupled to solid particles modelled using the approach introduced by Ladd and Aidun [29, 33–35] to investigate the validity and suitability of several analytical approximations of the bridge forces.

This paper is organized as follows. In Section II(A-B), we introduce some widely used models for the capillary bridge force. In section II(C), we describe the multicomponent lattice Boltzmann method that we use to model the capillary bridges forming between spherical particles. In Section III we investigate five different capillary bridge models with small and large bridge volumes, some of which have been frequently used to describe capillary bridge forces in Discrete Element Method (DEM) simulations [18, 36]. As an example of the possible applications, we use one of the potentials

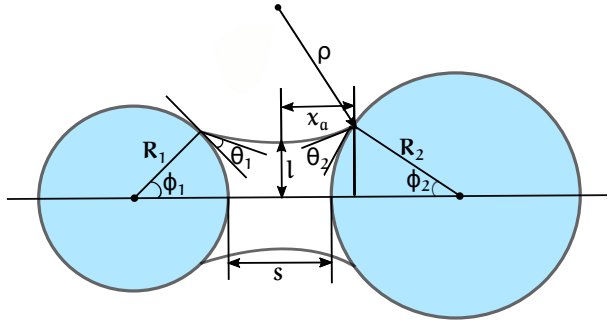


FIG. 1: Sketch of the liquid bridge geometry displaying the parameters involved in the calculations.

to model the interaction between particles and show the formation of clusters due to the capillary bridges under shear flow. In Section IV we discuss the limit of the theoretical models and summarize our results.

II. METHODOLOGY

A. Capillary bridge geometry and bridge volume

The volume of the liquid bridge is an important ingredient in the calculation of the capillary force and needs special attention. Fig. 1 depicts a sketch of the main geometrical quantities involved in the description of the bridge. Two particles of radius R_1 and R_2 , respectively, are separated by the surface-to-surface distance S . The principal radii of the liquid meniscus are ρ and l , respectively, and the volume of each particle is $V_{p,1}$ and $V_{p,2}$. The contact angles are denoted as θ_1 and θ_2 , and the half-filling angles are denoted as ϕ_1 and ϕ_2 . x_a and y_a are the abscissa and ordinate of the contact point between the solid and liquid profiles. The coordinate system is chosen such that the x -axis lies along the straight line joining the centers of the particles, with its origin located at the middle point between the spherical surface. By integrating the liquid profile $y(x)$ one can obtain the liquid volume of the bridge V_l , which in the case of two equal spheres reads

$$V_l = \pi \int_{-x_a}^{x_a} y^2(x) dx - 2V_s, \quad (1)$$

where V_s is the volume of the spherical caps wet by the liquid. The volume of the spherical caps

are calculated geometrically as $\pi R_1^3(2 + \cos \phi_1)(1 - \cos \phi_1)^2/3$ and $\pi R_2^3(2 + \cos \phi_2)(1 - \cos \phi_2)/3$, respectively. In the toroidal approximation, the meridional profile of pendular bridges is approximated by an arc of a circle. This approximation leads to a simple closed-form solution for the Young-Laplace equation, which has been widely used for the estimation of the forces between spherical particles [3, 17]. In this approach, the surface curvature is not constant along the meniscus of the liquid bridge. Consequently, the total force in the toroidal approximation is a function of the local surface curvature and thus of the position of the orthogonal plane [5]. The toroidal approximation can be used for small menisci, where the effect of gravity can be neglected. Deviations from the toroidal approximation agree with the results from the forces calculated numerically with the exact bridge shape [13]. Many authors used the toroidal approximation to calculate the liquid bridge volume for equally and unequally-sized spheres [7, 8, 15, 17, 37]. Pietsch and Rumpf reported the expression of the bridge volume with a wide range of partial wetting, as shown in Table I [37]. Other authors derived simpler expressions with further simplifications. However, their expressions underestimate [17, 38] or overestimate [6] the bridge volume, as compared to the values obtained in Refs. [7, 37]. Megias-Alguacil and Gauckler calculated the liquid bridge volume in terms of the abscissa x_a , the contact angle and the separation distance [7]. In case of two equal spheres, their expression is fully equivalent to the one from Pietsch and Rumpf if the relation

$$\phi = \arccos [S/(2R_p) + 1 - x_a/R_p] \quad (2)$$

is used [37]. Chen and coworkers developed an improved mechanical model which is capable of analyzing the force and the volume of the liquid bridge by assuming that the liquid bridge profile is circular in shape between two unequally-sized spherical particles [14]. Later, Sun and Sakai proposed a more general expression for the capillary bridge volume which coincides with the one of Chen and coworkers if the spheres have the same contact angle [15].

B. Capillary bridge force

The capillary force is usually calculated following one of two routes, namely, the geometric one (approximating the solution of the Laplace equation) and the energetic one (taking the derivative of the total interfacial energy). In the geometric approach,

the capillary force exerted on solid spheres due to the liquid bridge is the sum of two components, which are the contributions from the surface tension and the hydrostatic pressure, respectively. The surface tension and hydrostatic contributions can be obtained by knowing the height of the neck, the tangent of the profile and the contact area, respectively. The direction of the hydrostatic pressure force depends on the curvature of the meniscus, while the surface tension force is always attractive. Convex bridges yield positive Laplace pressure contributions and repulsive hydrostatic pressure forces. On the contrary, the pressure in concave bridges is negative, and the corresponding force attractive. Once the profile of the bridge is known, both terms can be determined by geometrical means. In this study, the capillary force is attractive for $F \downarrow 0$ and repulsive for $F \uparrow 0$.

In order to obtain the hydrostatic pressure in the geometric approach, the geometry of the bridge has to be approximated. The so-called toroidal and Derjaguin approximations are two widely applied options. For relatively small liquid bridges (mostly concave) and at stable separation distances, the toroidal approximation has been shown to produce errors smaller than 10% in the calculated capillary force, in comparison with exact numerical techniques [3, 39, 40]. However, with increasing separation distance, the toroidal solution may underestimate the capillary bridge force [41]. Alguacil and Gauckler studied the validity of the toroidal approximation for the case of convex liquid bridges, showing agreement within 30% with the numerical solution of the Young-Laplace equation [8, 42].

The Derjaguin approximation was originally developed for determining the force between unequal spheres based on the interaction energy between planar surfaces. The validity of this approximation is intuitively limited to separation distances that are small compared to the radii of the spheres, or, equivalently, when the radius of the bridge profile is orders of magnitude smaller than the neck radius. Rabinovich and coworkers found that Derjaguin's approximation is valid only at strictly zero separation distance [6]. Willett and coworkers proposed a variant of the Derjaguin approximation for the total capillary forces between spheres as a function of the separation distance and for a fixed bridge volume [5]. In the energetic approach, the total capillary force is obtained by perturbing the displacement S between the two particles, provided that the volume of the

Models	Capillary bridge volume V_l
Pietsch & Rumpf [37]	$\frac{V_l}{2\pi} = \rho(\rho^2 + b^2) \cos(\theta + \phi) - \frac{1}{3}\rho^3 \cos^3(\theta + \phi)$ $- \frac{1}{24}d_p^3(2 + \cos\phi)(1 - \cos\phi)^2$ $- b[\rho^2 \cos(\theta + \phi) \sin(\theta + \phi) + \rho^2 (\frac{\pi}{2} - \theta - \phi)]$ $b = \rho + l, \rho = \frac{d_p(1 - \cos\phi) + S}{2 \cos(\theta + \phi)}$ $l = R_p \sin\phi + \rho[\sin(\theta + \phi) - 1]$
Alguacil & Gauckler [7]	$\frac{V_l}{2\pi} = ((l - \rho)^2 + \rho^2)x_a - \frac{x_a^3}{3} + (l - \rho) \left[x_a \sqrt{\rho^2 - x_a^2} + \rho^2 \arcsin \frac{x_a}{\rho} \right]$ $- \frac{1}{3}(x_a - S/2)^2(3R_p - (x_a - S/2))$ $\rho = \frac{x_a R_p}{(S/2 + R_p - x_a) \cos\theta - \sqrt{R_p^2 - (x_a - S/2 - R_p)^2} \sin\theta}$ $l = \sqrt{R_p^2 - (x_a - S/2 - R_p)^2} + x \frac{\sqrt{R_p^2 - (x_a - S/2 - R_p)^2} \cos\theta + (S/2 + R_p - x_a) \sin\theta - R_p}{(S/2 + R_p - x_a) \cos\theta - \sqrt{R_p^2 - (x_a - S/2 - R_p)^2} \sin\theta}$
Chen et al.[14]	$V_1 = \pi\rho(a^2 + \rho^2)(\cos(\phi_1 + \theta) + \cos(\phi_2 + \theta)) - \frac{\pi}{3}\rho^3(\cos^3(\phi_1 + \theta) + \cos^3(\phi_2 + \theta)) - a\pi\rho^2(\sin(\phi_1 + \theta) \cos(\phi_1 + \theta) + \sin(\phi_2 + \theta) \cos(\phi_2 + \theta) + a\rho^2(\phi_1 + \phi_2 + 2\theta - \pi))$ $V_2 = \frac{\pi}{3}((2 - 3 \cos\phi_1 + \cos^3\phi_1)R_1^3 + (2 - 3 \cos\phi_2 + \cos^3\phi_2)R_2^3)$ $V_l = V_1 - V_2$ $\rho = \frac{R_1(1 - \cos\phi_1) + S + R_2(1 - \cos\phi_1)}{\cos(\phi_1 + \theta) + \cos(\phi_2 + \theta)}$ $l = R_1 \sin\phi_1 - \rho(1 - \sin(\phi_2 + \theta))$

TABLE I: Capillary bridge volume (V_l) from different theoretical models

liquid is constant

$$F = \frac{dW}{dS}, \quad (3)$$

where W is the interfacial free energy determined by surface tension, interface contact areas and contact angle [43]. Rabinovich and coworkers showed that the energetic and geometric routes are equivalent despite the nonequilibrium nature of the problem, and proposed an explanation for the failure of the Derjaguin approximation at large distances [6]. Chau and coworkers calculated the capillary force for non-axisymmetrical shapes allowing the meniscus to fulfill the Kelvin equation [44]. More recently, Wang and coworkers used the interfacial energy minimization approach to study the forces and the rupture behaviour of water bridges between three spherical particles at equilibrium configurations [45].

In the following we consider five different theoretical models, which are representative of the bulk of works on the subject. Theoretical models have limitations due to the approximations made in solving the Young-Laplace equation. To gain insight into different models, we explore the quality of the models for the prediction of capillary bridges using our lattice Boltzmann simulations.

In model A, as reported by Lian and coworkers, the liquid bridge force is calculated by the toroidal approximation [3]. We use the “gorge” method ($F = \pi l^2 \Delta p + 2\pi\sigma l$) from their work, in which the area at the neck is used to calculate

the hydrostatic pressure force and the tangent at the neck to obtain the surface tension force. The capillary force is calculated in terms of the half-filling angle, separation distance, and contact angle. For a wide range of liquid bridge volumes and stable separation distances, this method produces errors within 10% in the calculation of the capillary force in comparison with <https://latex.hiern.de/project/5e565d1c2ef5060157deb605> those obtained from an exact numerical technique.

Model B was used by several authors, deriving the expression for the capillary force by the toroidal approximation [7, 17, 37]. In this model, the surface tension force ($2\pi\sigma R_p \sin\phi \sin(\phi + \theta)$) is obtained at the intersection of the three-phase contact line; and the hydrostatic pressure force is calculated by the axially projected wetted area of the particle. In Model B, the capillary force depends on the half-filling angle, separation distance, and contact angle.

Model C is a semi-analytical model proposed by Willett and coworkers [5]. The volume of the capillary bridge is in this case an input of the problem and, in the following comparison, we will use the value obtained from the simulations. The error of their approximations is no more than 4% when the liquid-to-solid volume ratio is 0.001. However, the error increases with increasing volume ratio. The accuracy can be improved with a more complex expression, which is valid for half-filling angles $< 50^\circ$ and volume ratios V^* less than 0.1, giving an error

in the force estimation of less than 3%. Model C can also be used to calculate the total capillary force for unequal spheres. The authors pointed out that deviations from the solution for equal spheres occur only when the bridge volume is large compared to that of the spheres.

Model D represents the approach of Rabinovich and coworkers, who obtained the capillary force between two spheres based on the Derjaguin approximation [6]. Model E is from Miakmi and coworkers, who derived a formula for the liquid bridge force as an explicit function of the liquid bridge volume and separation distance based on the regression analysis of the numerical solutions of the Young-Laplace equation [4]. The details of the models can be found in Table II. Again, like in the case of Model C, for both Model D and Model E, the liquid bridge volume is an input of the problem.

C. Lattice Boltzmann Method

The lattice Boltzmann method is a mesoscopic approach to approximate solutions of the Navier-Stokes equations by computing the moments of the Boltzmann transport equation solved on a lattice [46]. Here, we model the droplet using the multicomponent lattice Boltzmann method of Shan and Chen [27, 32]. Each component follows a discretized Boltzmann equation

$$f_i^c(\vec{x} + \vec{c}_i \Delta t, t + \Delta t) = f_i^c(\vec{x}, t) + \Omega_i^c(\vec{x}, t), \quad (4)$$

where $f_i^c(\vec{x}, t)$ represent the amount of particles of component c at lattice position \vec{x} and at time t that are moving along the i -th of the $N = 19$ discretized directions, with velocity $\vec{c}_i (i = 1, \dots, N)$ commensurate with the three-dimensional lattice. In reduced units, the timestep Δt and the lattice constant Δx are set to 1. Here, Ω_i^c is the Bhatnagar-Gross-Krook (BGK) collision operator representing the relaxation of the particle distribution towards the local Maxwell-Boltzmann equilibrium [47]

$$\Omega_i^c = -\frac{f_i^c(\vec{x}, t) - f_i^{eq}[\rho^c(\vec{x}, t), \vec{u}^c(\vec{x}, t)]}{\tau^c}, \quad (5)$$

where the equilibrium distribution is approximated as

$$f_i^{eq} = \zeta_i \rho^c \left[1 + \frac{\vec{c}_i \vec{u}}{c_s^2} + \frac{(\vec{c}_i \vec{u})^2}{2c_s^4} - \frac{u^2}{2c_s^2} \right]. \quad (6)$$

Here, τ^c sets the relaxation time. $\rho_c(\vec{x}, t) = \rho_0 \sum_i f_i^c(\vec{x}, t)$ is the fluid density, and $\vec{u} = \vec{u}^c(\vec{x}, t)$

(defined by $\rho_c(\vec{x}, t) \vec{u}^c(\vec{x}, t) \equiv \sum_i f_i^c(\vec{x}, t) \vec{c}_i$) is the macroscopic bulk velocity of the fluid. ρ_0 is a reference density and is chosen to be 1. $c_s = 1/\sqrt{3}$ is the speed of sound and ζ_i are the coefficients from the velocity space discretization. $\nu_c = c_s^2(\tau_c - 1/2)$ is the kinematic viscosity of the fluid.

The fluid interaction between components c and c' is

$$\vec{F}^c(\vec{x}, t) \equiv -\Phi^c(\vec{x}, t) \sum_{c'} G_{cc'} \sum_{\vec{x}'} \Phi^{c'}(\vec{x}', t) (\vec{x}' - \vec{x}), \quad (7)$$

where \vec{x}' are the nearest neighboring lattice sites. $\Phi^c(\vec{x}, t)$ is the effective mass and we use

$$\Phi^c(\vec{x}, t) = \rho_0 \left[1 - \exp \left(-\frac{\rho^c(\vec{x}, t)}{\rho_0} \right) \right]. \quad (8)$$

$G_{cc'}$ represents the coupling-constant of the interaction potential between components c and c' . In this work, we use $G_{cc'} = 0.1$. The effect of the force is imposed by adding a shift to the velocity \vec{u} in the equilibrium distribution

$$\Delta \vec{u}^c(\vec{x}, t) = \frac{\tau^c \vec{F}^c(\vec{x}, t)}{\rho^c(\vec{x}, t)}. \quad (9)$$

The actual macroscopic bulk velocity is finally calculated as

$$\rho^c(\vec{x}, t) \vec{u}^c(\vec{x}, t) = \sum_i f_i^c(\vec{x}, t) \vec{c}_i + \frac{\vec{F}^c(\vec{x}, t)}{2}. \quad (10)$$

The particles are discretized on the fluid lattice and interactions between the fluid and the particles are introduced using a modified bounce-back boundary condition, resulting in a modified lattice Boltzmann equation [29, 34]. The particles follow Newton's equations of motion for the linear and angular momentum

$$\vec{F}_p = m \frac{d\vec{u}_p}{dt} \quad (11)$$

$$\vec{D} = J \frac{d\vec{\omega}}{dt}, \quad (12)$$

where \vec{F} is the total force acting on a particle, m is the particle mass, and \vec{u}_p its velocity. \vec{D} is the torque, J the particle's moment of inertia, and $\vec{\omega}$ its angular velocity.

The force in Eq. 7 considers interactions between a lattice node outside of a particle and a lattice node inside a particle. To calculate these interactions, we

Models	Capillary force F
Model A	$F = 2\pi\sigma l \left(1 + \frac{l-\rho}{2\rho}\right)$
Lian et al.[3]	$\rho = \frac{2R_p(1-\cos\phi)+S}{2\cos(\theta+\phi)}$ $l = R_p \sin\phi - (R_p(1-\cos\phi) + S/2) \frac{1-\sin(\theta+\phi)}{\cos(\theta+\phi)}$
Model B	$F = 2\pi R_p \sigma \sin\phi \sin(\theta + \phi) + \pi\sigma R_p^2 \sin^2\phi \left(\frac{1}{\rho} - \frac{1}{l}\right)$
Huppmann[17], Pietsch[37]	$\rho = \frac{2R_p(1-\cos\phi)+S}{2\cos(\theta+\phi)}$ $l = R_p \sin\phi - (R_p(1-\cos\phi) + S/2) \frac{1-\sin(\theta+\phi)}{\cos(\theta+\phi)}$
Model B	$F = 2\pi\sigma R_p \sin\phi \sin(\phi + \theta) - \pi R_p^2 \sigma \sin^2\phi \left(\frac{1}{l} + \frac{1}{\rho}\right)$
Megias & Gauckler[8]	$\rho = \frac{x_a R_p}{\sqrt{R_p^2 - (x_a - S/2 - R_p)^2} \sin\theta - (S/2 + R_p - x_a) \cos\theta}$ $l = \sqrt{R_p^2 - (x_a - S/2 - R_p)^2} +$ $+ x_a \frac{\sqrt{R_p^2 - (x_a - S/2 - R_p)^2} \cos\theta + (S/2 + R_p - x_a) \sin\theta - R_p}{(S/2 + R_p - x_a) \cos\theta - \sqrt{R_p^2 - (x_a - S/2 - R_p)^2} \sin\theta}$
Model C	$F = 2\pi R_p \sigma \exp \left[f_1 - f_2 \exp \left(f_3 \ln \frac{S}{2\sqrt{V/R_p}} + f_4 \ln^2 \frac{S}{2\sqrt{V/R_p}} \right) \right]$
Willett et al.[5]	
Model D	$F = \frac{2\pi\sigma R_p \cos\theta}{1+S/(2d)}$
Rabinovich et al.[6]	$d = \frac{S}{2}(-1 + \sqrt{1 + 2V_l/(\pi R_p S^2)})$
Model E	$F^* = \exp(AS^* + B) + C$
Mikami et al.[4]	$A = -1.1\bar{V}^{-0.53}$ $B = (-0.34 \ln \bar{V} - 0.96)\theta^2 - 0.019 \ln \bar{V} + 0.48$ $C = 0.0042 \ln \bar{V} + 0.078$ $\bar{V} = \frac{4\pi}{3}V^*$

TABLE II: Capillary force from different theoretical models (the definitions of the coefficients f_1, f_2, f_3 and f_4 are presented in the Supplementary Material). Note that the two expressions reported for Model B found in the literature are equivalent. In original models B (Megias & Gauckler[8]) and D, negative capillary forces indicate attraction whereas a positive force is repulsive. To keep consistency with our current study, we use positive capillary forces from models B and D for attraction.

fill the lattice nodes in the outer shell of the particle with a virtual fluid. We define a parameter $\Delta\rho$, the particle colour, which allows us to control the interaction between the particle surface and the two fluids as

$$\rho_{virt}^r(\vec{x}, t) = \rho^r(\vec{x}, t) + |\Delta\rho| \quad (13)$$

$$\rho_{virt}^b(\vec{x}, t) = \rho^b(\vec{x}, t) - |\Delta\rho|, \quad (14)$$

where $\rho_{virt}^r(\vec{x}, t)$ and $\rho_{virt}^b(\vec{x}, t)$ are the averages of the densities of neighboring fluid nodes for components r and b , respectively. A particle color $\Delta\rho = 0$ corresponds to a contact angle of $\theta = 90^\circ$, i.e., a neutrally wetting particle [48, 49].

We place two particles ($R_p = 80$ lattice units for equal spheres, $R_p = 70$ and 90 lattice units, respectively, for unequally sized spheres) along the x axis, separated by a surface-to-surface distance S . A droplet is initialized in the center of the system. The droplet size is chosen large enough to make sure

that the capillary bridge can form between two particles (a minimum droplet radius of 23 lattice sites is used). As constant input parameters, we prescribe the liquid bridge volume $V_l = V_{bridge}$, the contact angle θ , the particle-particle separation distance S and the surface tension of the fluid, σ . By changing the droplet radius and length, we can obtain a wide range of liquid-to-solid volume ratios. We fix the position and orientation of the particles and let the system equilibrate. Then, we measure the forces acting on the particles for different values of the separation, contact angle, and volume ratio. To study the effect of discretization artefacts, we carried out a convergence study for the capillary force calculation, as a function of the grid size. In these tests, the relative liquid bridge volume is fixed at 0.133, and the effective resolution is increased by employing larger particle radii and correspondingly a higher number of lattice sites. Table III summarizes the calculated capillary force. By increasing the resolution by a factor of three, the change in force is only about 2.5%.

This value can be therefore used as an estimate of the (quite small) discretization error.

If not specified otherwise, we present all results in dimensionless units. The dimensionless force, bridge volume and separation distance are defined as $F^* = \frac{F}{\sigma R_p}$, $V^* = \frac{V_l}{V_p}$, and $S^* = \frac{S}{R_p}$.

III. RESULTS AND DISCUSSION

We vary the ratio of bridge volume to particle volume $V^*(V_l/V_p)$ from 0.07 to 0.7. The dimensionless separation distance $S^*(S/R_p)$ between spheres is changed from 0.25 to 1.45 to obtain the corresponding liquid bridge force. The influence of the contact angle is tested by performing simulations for $\theta = 34.6^\circ, 48^\circ, 60^\circ$ and 74° , respectively.

We report the bridge profiles under different liquid volumes and contact angles in Fig. 2 using the same liquid volume $V^* = 0.133$. As expected, the bridge shape is symmetric. However, one can appreciate that the meniscus changes from concave to convex when the liquid volume is increased. This change is induced by the geometric constraints, even though the wetting parameter (defining the contact angle of a droplet on a plane surface) is kept constant.

In Fig. 3 we compare the force/distance relation obtained with the lattice Boltzmann method to the predictions of the theoretical models at various contact angles. A similar behaviors are observed at different bridge volumes, and reported in the Supplementary Material).

Models A, B and C show a very good qualitative and quantitative agreement with the simulation results, with relatively small discrepancies ($< 10\%$), nicely reproducing the different trends characterizing the different contact angles. Models A and B predict slightly higher capillary forces than calculated with the lattice Boltzmann simulation, while model C predicts slightly lower values. Models D and E are both qualitatively and quantitatively not satisfactory, showing a slope of the force/distance curve that is only mildly dependent on the contact angle. While Model D partly underestimates and partly overestimates the capillary bridge force, Model E constantly overestimates it by a factor 1.5 to 3.

The overall trend indicates the capillary force decreasing with increasing particle separation, due to the decreasing surface tension force. When the contact angle or the bridge volume increase, the slope of the force/distance curve decreases. And at $\theta = 60^\circ$ or $V^* = 0.25$ (see Fig 4b), the capillary

force/distance curve becomes almost flat, except for the appearance of a maximum at a reduced separation distance $S/R_p \simeq 0.5$. In this case, the bridge profile is convex at small separation S while it becomes concave at large S . The peak displayed by the capillary force, previously already reported [7, 50], originates from the non-monotonic Laplace component [7].

Next, we present results on capillary bridges between two static unequally sized spheres with identical contact angles. There is limited work in the literature regarding spheres of different size. Chen and coworkers (and later Sun and Sakai [15]) proposed a mechanical model to analyze the force and the volume of the liquid bridge, by considering a circular arc-shaped liquid bridge profile between two unequally sized spheres [14]. In the following, we denote these models as Model F, and we provide a comparison of its predictions with the results of our lattice Boltzmann simulations. In addition, we show the predictions of Model C, computed using the harmonic mean of the radii $R_m = \frac{2R_1R_2}{R_1+R_2}$ to calculate capillary forces and bridge volumes [5]. In the simulations and model F, we use $R_p = 70$ and 90 lattice units, respectively.

In Fig 5 we report the force/distance curves for unequal spheres. The behavior is qualitatively similar to the equal sphere case. At moderate contact angles and liquid volumes, the capillary force decreases with increasing particle separation due to the decreasing surface tension force, and a maximum in the force appears for the largest contact angle and liquid volume considered, much like in the symmetric system.

Model F captures qualitatively very well the trend of the force/distance curves, also at high contact angles and liquid bridge volumes, and is also quantitatively accurate under most conditions. Model C is worse than Model F in reproducing the qualitative trend at high contact angles and high liquid bridge volumes. However, from the quantitative point of view, Model C and Model F provide, on average, comparable predictions.

In the Supplementary Material, we also report the predictions of Models C and F, where we use, again, the harmonic mean of the radii.

The results presented above show that several models have problems in reproducing the force/separation curves when the liquid bridge volume starts becoming comparable with that of the solid particles. The capillary bridge volume has an influence on the bridge shape (and consequently on the force) has also been demonstrated by experi-

Box size	$F/(\sigma R_p)$
$128 \times 128 \times 248$	1.92
$192 \times 192 \times 336$	1.94
$256 \times 256 \times 448$	1.94
$384 \times 384 \times 608$	1.97

TABLE III: Dimensionless capillary force ($F/(\sigma R_p)$) calculated from LBM-DEM at $R_p/N_x = 0.3125$, $S/R_p = 0.625$ and $V_l/V_p = 0.133$.

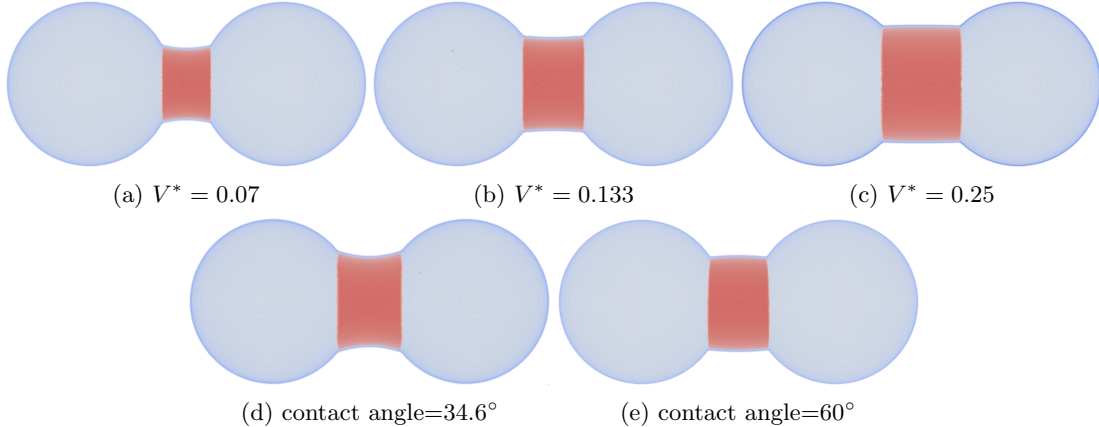


FIG. 2: Liquid bridge profile with different volume ratios under fixed separation distance ($S/R_p = 0.375$) (top row: contact angle $= 48^\circ$) and contact angles (bottom row: volume ratio $V^* = 0.133$).

ments [19]. In fact, at high volumes or contact angles, as reported by Niven, liquid bridges tend even to adopt non-axisymmetric geometries [51]. The lattice Boltzmann simulations can also reproduce this condition. Fig. 6 illustrates the appearance of an asymmetric liquid bridge (e.g. tear-drop shape) between spheres at different contact angles and bridge volumes. A droplet sits initially between two fixed particles. Then it migrates from its axisymmetric configuration to one side due to the pressure gradient produced from the top and bottom curvatures. In the case of the highest contact angle (132°) a mechanically stable state is reached, and the capillary force is zero, whereas for neutral wetting conditions ($\theta = 90^\circ$), we measure non-zero attractive forces. Clearly, these configurations cannot be described by the models discussed here. Interestingly, however, models A, B, C and D would predict a transition from attractive to repulsive capillary forces.

Many particles system under shear flow

Model C predicts the capillary force with high accuracy, and is also easy to be implemented in a DEM

code. To show the possibilities opened by coarse-graining the capillary interaction using this simple model potential, we run several LBM/DEM simulations of a suspension of particles in a shear flow, and study the influence of the presence and strength of the capillary bridge on the structural properties of the wet granular material.

Our starting configurations are generated by placing 2000 particles (with radius $R_p = 3\Delta x$) randomly in a cubic simulation box (side length of $128\Delta x$). This corresponds to a packing fraction of 10%. We assume that the secondary fluid is, effectively, uniformly distributed among all the particles with a constant fraction of 5×10^{-6} .

Capillary bridge forces are introduced using model C and, consequently, the dynamics of the secondary fluid is not resolved in these simulations. The contact angle parameter is set to 123 degrees. We obtain different degrees of capillary bridge strength by changing the surface tension coefficient. The shear flow is imposed using Lees-Edwards boundary conditions [52, 53] in the x -direction, generating a spatially homogeneous, linear shear flow. The usual periodic boundary conditions with no imposed velocity are applied to the remaining directions.

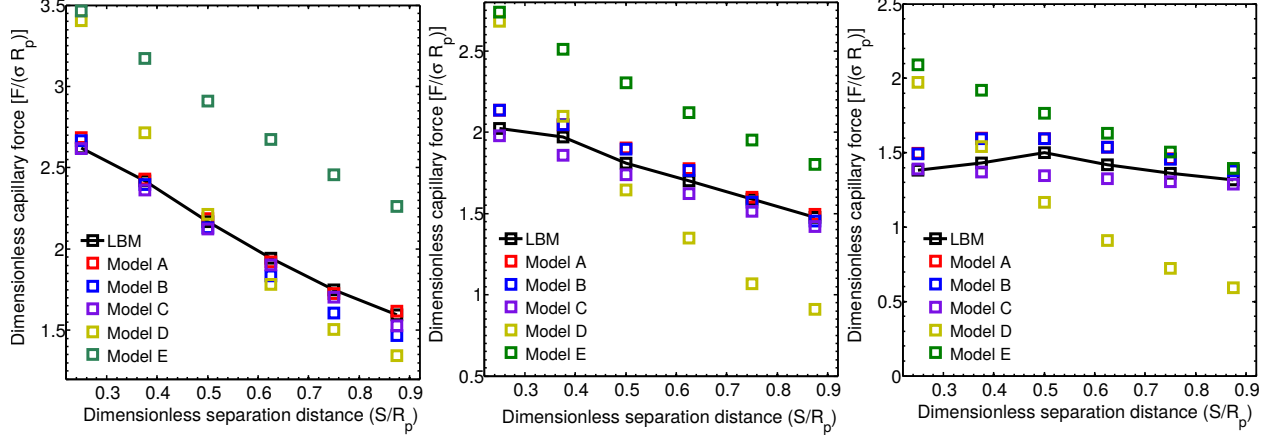


FIG. 3: Capillary bridge force between two equally-sized spheres with bridge volume $V^* = 0.133$, for different contact angles (left panel: 34.6° , middle panel: 48° , right panel: 60°).

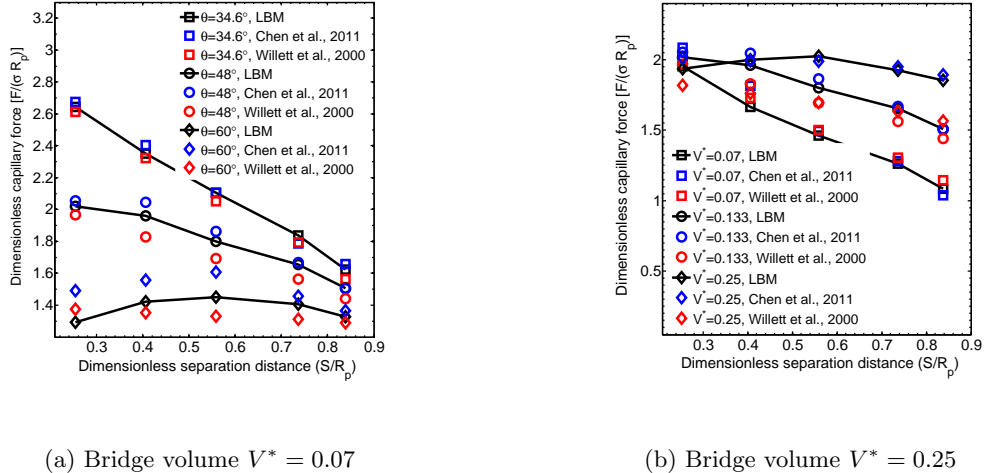


FIG. 4: Dimensionless capillary bridge force ($F/(\sigma R_p)$) between two equal spheres under different bridge volume. (Contact angle $\theta = 48^\circ$)

In Fig 7, we present instantaneous snapshots of the system, showing the formation of particle clusters due to capillary bridges. We colour the particles based on a simple cutoff clustering algorithm, as implemented in the Pytim software package [54]. Two particles are assigned to the same cluster if their distance is less than the cutoff $\delta_r = 6.5\Delta x$ (the radius of particles being $3.0\Delta x$). Without capillary bridge forces (Fig 7a), particles are homogeneously distributed in the system. With weak capillary bridge forces (Fig 7b), only a limited tendency to cluster formation is observed. The aggregating force is balanced by the presence of shear, that tends to disrupt

the clusters. With stronger capillary forces (Figs 7c and 7d), the shear forces are not anymore able to prevent the formation of clusters, and increasingly large structures are found.

To provide a more quantitative picture, in Fig 8 we report the histograms of the cluster size distribution, sampled over the time span from 10^6 to $4 \times 10^6 \Delta t$, after having reached stationary conditions. Without capillary force (Fig 8a), around 80% of the particles do not belong to any cluster (cluster size equal one), and the largest cluster observed is composed of 8 particles. With increasing capillary force (Figs 8b-d), an increasing amount of particles is involved in

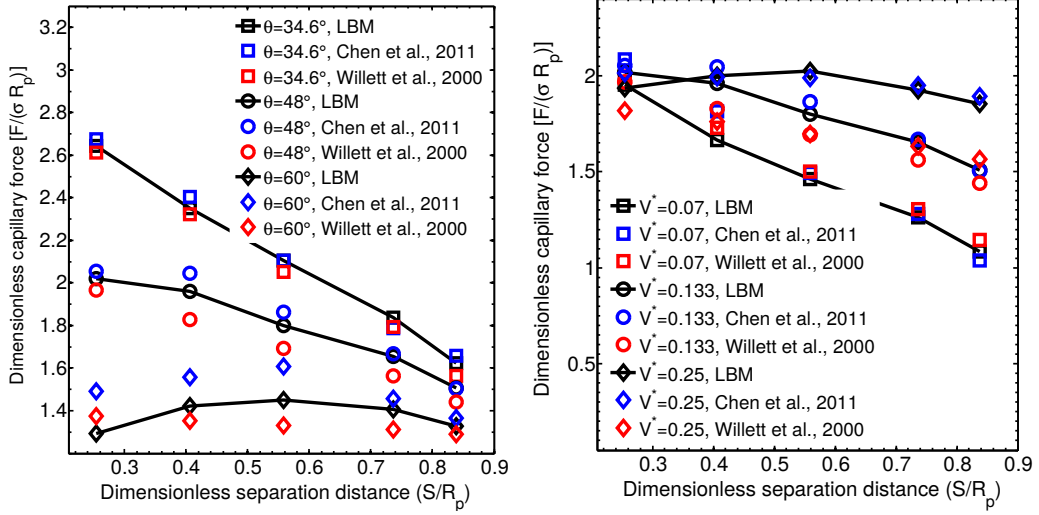


FIG. 5: Capillary bridge force between two unequally-sized spheres with radii equal to 70 and 90 lattice units, respectively. Left panel: different contact angles and bridge volume $V^* = 0.133$. Right panel: different bridge volumes and the same contact angle $\theta = 48^\circ$.

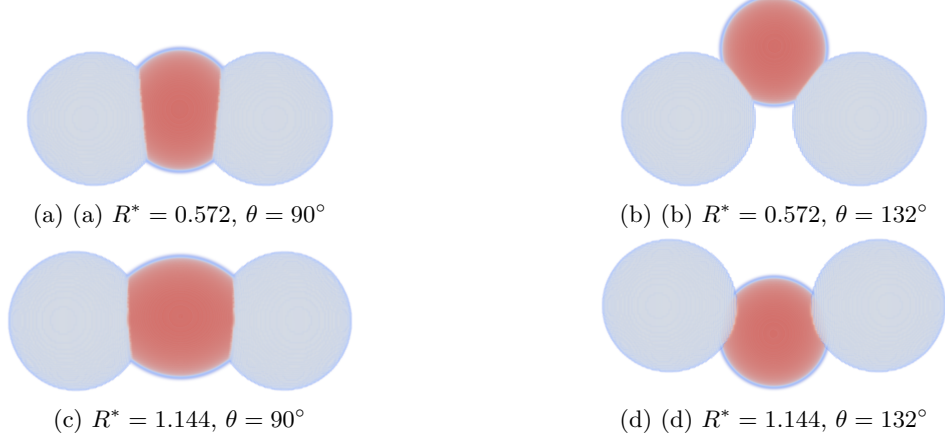
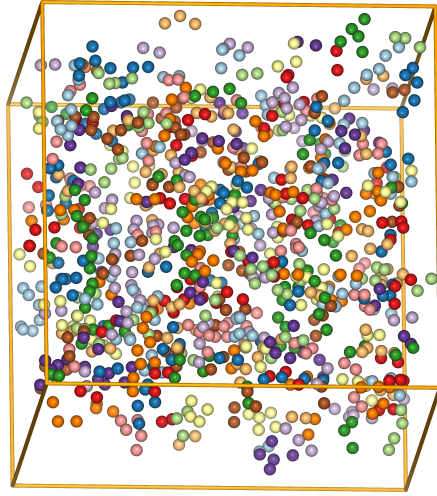


FIG. 6: Asymmetric liquid bridge between equal spheres from lattice Boltzmann simulation at different separation distances ($V^* = 0.5$ for $S^* = 0.572$, $V^* = 0.65$ for $S^* = 1.144$)

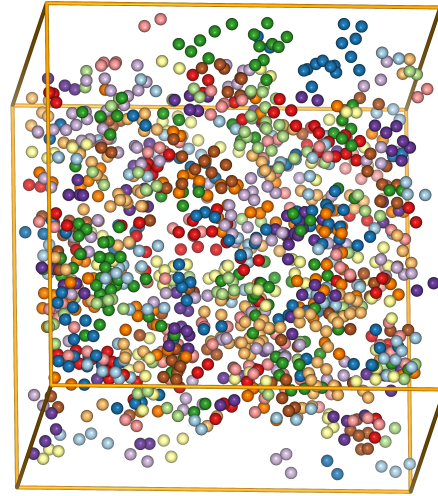
larger clusters and eventually, particles tend to agglomerate in a single cluster (Fig 8d, the average size of the largest cluster containing 850 particles). In this case, the particles not belonging to any cluster are just a small fraction (5-6%) of the total number of clusters.

CONCLUSION

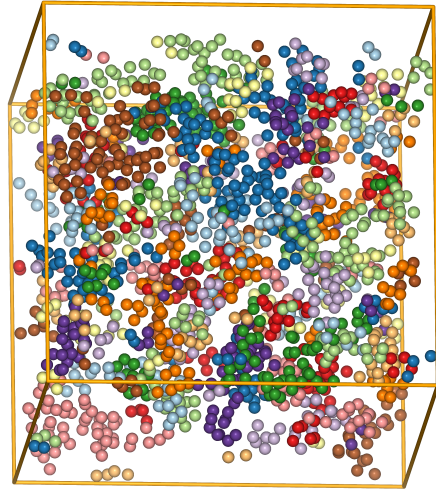
We performed lattice Boltzmann numerical simulations of the static capillary bridge between equally and unequally-sized spherical particles at different wetting conditions and liquid bridge volumes. We reviewed some of the most popular analytical and semi-analytical models that predict the capillary bridge force between particles and compared them to the results of the numerical simulations, to explore



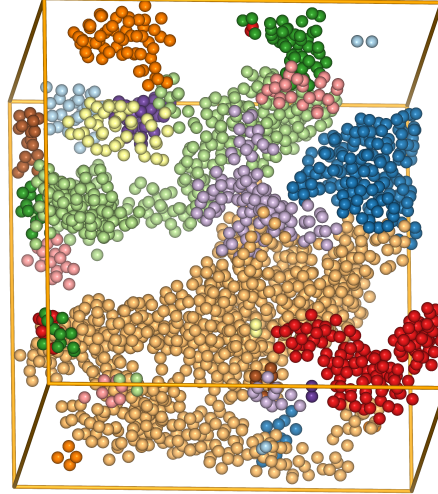
(a) No capillary force



(b) $\sigma = 1 \times 10^{-5}$



(c) $\sigma = 5 \times 10^{-5}$



(d) $\sigma = 5 \times 10^{-4}$

FIG. 7: Simulation snapshots of particle clustering at $t = 4 \times 10^6 \Delta t$ under different capillary forces in a shear flow. Particles belonging to the same cluster have the same color. (a: no capillary force; b,c,d: capillary force with different surface tension parameter σ).

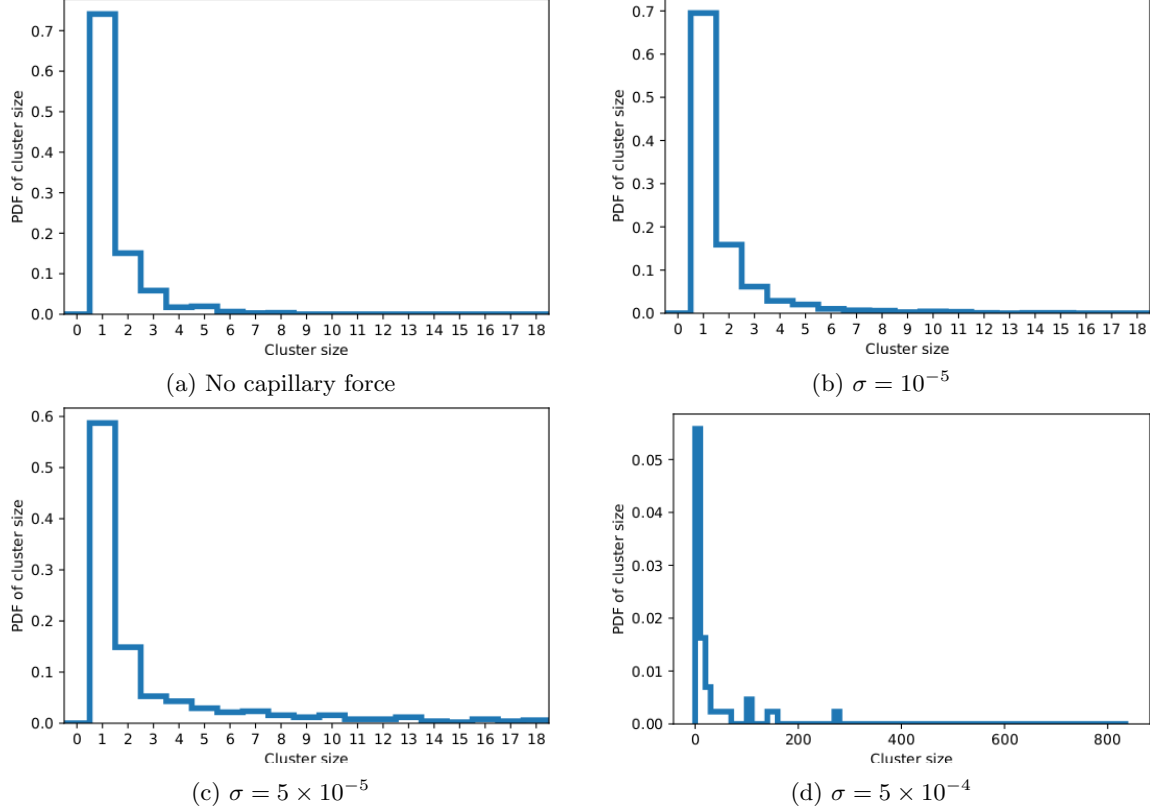


FIG. 8: Particle cluster size (i.e., the total number of particles in a cluster) distribution in a time span from 10^6 to $4 \times 10^6 \Delta t$. Clusters form due to the presence of capillary bridges between the suspended particles in a shear flow (a: no capillary bridges force; b,c,d: capillary force with different surface tension parameter σ).

their validity and suitability for modeling capillary bridges forces.

For pairs of equally-sized spherical particles, sufficiently small contact angles and liquid-to-solid volume ratios, three models are found to be in good qualitative and quantitative agreement with the numerical simulations. In case of unequal spherical particles, the model of Willett and coworkers [5] (Model C), as well that of Chen and coworkers [14] (Model F) turned out to describe reasonably well the capillary bridge force, also at moderately high contact angles and volume fractions. In this sense, both models are good candidates to implement capillary forces in discrete element method simulations.

As an example of a possible application, we showed the capability of model C to study the influence of the capillary bridge force on the agglomeration of particles in a shear flow. Up to moderate capillary force strengths, the imposed shear flow is able to disrupt the forming clusters, but with stronger interactions one observes the transition to an almost

complete agglomeration.

This work lays the foundation of future investigations on the formation and rheology of large-scale systems of capillary-bridge agglomerates, thanks to the reduced computational requirement of the coarse-grained model. Possible future extensions of the current work include the modelling of asymmetric bridges, which form at high contact angles, and the inclusion of liquid transport across the bridges.

ACKNOWLEDGEMENT

The authors thank B. Nun, T. Plankenbühler and J. Karl for fruitful discussions. Financial support by the German Research Foundation (DFG) within the project HA 4382/7-1 as well as the computing time granted by the Jülich Supercomputing Centre (JSC) are highly acknowledged.

APPENDIX

The definitions of the coefficients f_1, f_2, f_3 and f_4 in Table II for model C are in Table IV.

[1] Herminghaus S. Dynamics of wet granular matter. *Advances in Physics* 2005; 54: 221.

[2] Gatternig B, Karl J. Investigations on the mechanisms of ash-induced agglomeration in fluidized-bed combustion of biomass. *Energy & Fuels* 2015; 29(2): 931–941.

[3] Lian G, Thornton C, Adams MJ. A theoretical study of the liquid bridge forces between two rigid spherical bodies. *Journal of Colloid and Interface Science* 1993; 161(1): 138–147.

[4] Mikami T, Kamiya H, Horio M. Numerical simulation of cohesive powder behavior in a fluidized bed. *Chemical Engineering Science* 1998; 53(10): 1927–1940.

[5] Willett CD, Adams MJ, Johnson SA, Seville JP. Capillary bridges between two spherical bodies. *Langmuir* 2000; 16(24): 9396–9405.

[6] Rabinovich YI, Esayanur MS, Moudgil BM. Capillary forces between two spheres with a fixed volume liquid bridge: theory and experiment. *Langmuir* 2005; 21(24): 10992–10997.

[7] Megias-Alguacil D, Gauckler LJ. Capillary forces between two solid spheres linked by a concave liquid bridge: Regions of existence and forces mapping. *AICHE Journal* 2009; 55(5): 1103–1109.

[8] Megias-Alguacil D, Gauckler LJ. Analysis of the capillary forces between two small solid spheres binded by a convex liquid bridge. *Powder Technology* 2010; 198(2): 211–218.

[9] Lambert P, Chau A, Delchambre A, Régnier S. Comparison between two capillary forces models. *Langmuir* 2008; 24(7): 3157–3163.

[10] Haines WB. Studies in the physical properties of soils: II. A note on the cohesion developed by capillary forces in an ideal soil. *The Journal of Agricultural Science* 1925; 15(4): 529–535.

[11] Fisher RA. On the capillary forces in an ideal soil; correction of formulae given by WB Haines. *The Journal of Agricultural Science* 1926; 16(3): 492–505.

[12] Derjaguin B. Untersuchungen über die Reibung und Adhäsion, IV. *Kolloid-Zeitschrift* 1934; 69(2): 155–164.

[13] Butt HJ, Kappl M. Normal capillary forces. *Advances in Colloid and Interface Science* 2009; 146(1–2): 48–60.

[14] Chen Y, Zhao Y, Gao H, Zheng J. Liquid bridge force between two unequal-sized spheres or a sphere and a plane. *Particuology* 2011; 9(4): 374–380.

[15] Sun X, Sakai M. A liquid bridge model for spherical particles applicable to asymmetric configurations. *Chemical Engineering Science* 2018; 182: 28–43.

[16] Lian G, Seville J. The capillary bridge between two spheres: New closed-form equations in a two century old problem. *Advances in Colloid and Interface Science* 2016; 227: 53–62.

[17] Huppmann WJ, Rieger H. Modelling of rearrangement processes in liquid phase sintering. *Acta Metallurgica* 1975; 23(8): 965–971.

[18] Roy S, Singh A, Luding S, Weinhart T. Micro-macro transition and simplified contact models for wet granular materials. *Computational Particle Mechanics* 2016; 3(4): 449–462.

[19] Farmer TP, Bird JC. Asymmetric capillary bridges between contacting spheres. *Journal of Colloid and Interface Science* 2015; 454: 192–199.

[20] Xiao F, Jing J, Kuang S, Yang L, Yu A. Capillary forces on wet particles with a liquid bridge transition from convex to concave. *Powder Technology* 2020.

[21] Vogel TI. Convex, rotationally symmetric liquid bridges between spheres. *Pacific Journal of Mathematics* 2006; 224(2): 367–377.

[22] Erle MA, Dyson DC, Morrow NR. Liquid bridges between cylinders, in a torus, and between spheres. *AICHE Journal* 1971; 17(1): 115–121.

[23] Brakke KA. The surface evolver. *Experimental mathematics* 1992; 1(2): 141–165.

[24] Rider WJ, Kothe DB. Reconstructing volume tracking. *Journal of computational physics* 1998; 141(2): 112–152.

[25] Sussman M, Smereka P, Osher S, others. *A level set approach for computing solutions to incompressible two-phase flow*. PhD thesis. Department of Mathematics, University of California, Los Angeles, 1994.

[26] Krüger T, Kusumaatmaja H, Kuzmin A, Shardt O, Silva G, Vignen EM. *The Lattice Boltzmann Method*. Springer . 2017.

[27] Liu H, Kang Q, Leonardi CR, et al. Multiphase lattice Boltzmann simulations for porous media applications. *Computational Geosciences* 2016; 20(4): 777–805.

[28] Brakke KA. Surface evolver manual. *Mathematics Department, Susquehanna University, Selinsgrove, PA* 1994; 17870(2.24): 20.

[29] Ladd AJC. Numerical simulations of particulate suspensions via a discretized Boltzmann equation. Part 1. Theoretical foundation. *Journal of Fluid Mechanics* 1994; 271: 285–309.

Coefficients	Expressions
f_1	$(-0.44507 + 0.050832\theta - 1.1466\theta^2)$ $-(0.1119 + 0.000411\theta + 0.1490\theta^2) \ln \bar{V}$ $-(0.012101 + 0.0036456\theta + 0.01255\theta^2)(\ln \bar{V})^2$ $-(0.0005 + 0.0003505\theta + 0.00029076\theta^2)(\ln \bar{V})^3$
f_2	$(1.9222 - 0.57473\theta - 1.2918\theta^2)$ $-(0.0668 + 0.1201\theta + 0.22574\theta^2) \ln \bar{V}$ $-(0.0013375 + 0.0068988\theta + 0.01137\theta^2)(\ln \bar{V})^2$
f_3	$1.268 - 0.01396\theta - 0.23566\theta^2$ $+(0.198 + 0.092\theta - 0.06418\theta^2) \ln \bar{V}$ $+(0.02232 + 0.02238\theta - 0.009853\theta^2)(\ln \bar{V})^2$ $+(0.0008585 + 0.001318\theta - 0.00053\theta^2)(\ln \bar{V})^3$
f_4	$-0.010703 + 0.073776\theta - 0.34742\theta^2$ $+(0.03345 + 0.04543\theta - 0.09056\theta^2) \ln \bar{V}$ $+(0.0018574 + 0.004456\theta - 0.006257\theta^2)(\ln \bar{V})^2$

TABLE IV: Coefficients f_1, f_2, f_3 and f_4 in Table II for Model C ($\bar{V} = \frac{4\pi}{3}V^*$)

- [30] Ahlrichs P, Dünweg B. Simulation of a single polymer chain in solution by combining lattice Boltzmann and molecular dynamics. *The Journal of Chemical Physics* 1999; 111(17): 8225–8239.
- [31] Segal M, Sbragaglia M, Kantorovich SS, Ivanov AO. Mesoscale structures at complex fluid–fluid interfaces: a novel lattice Boltzmann/molecular dynamics coupling. *Soft Matter* 2013; 9(42): 10092–10107.
- [32] Shan X, Chen H. Lattice Boltzmann model for simulating flows with multiple phases and components. *Physical Review E* 1993; 47(3): 1815.
- [33] Ladd AJC, Verberg R. Lattice-Boltzmann simulations of particle-fluid suspensions. *Journal of Statistical Physics* 2001; 104(5-6): 1191–1251.
- [34] Aidun CK, Lu Y, Ding E. Direct analysis of particulate suspensions with inertia using the discrete Boltzmann equation. *Journal of Fluid Mechanics* 1998; 373: 287–311.
- [35] Harting J, Frijters S, Ramaioli M, Robinson M, Wolf DE, Luding S. Recent advances in the simulation of particle-laden flows. *European Physical Journal Special Topics* 2014; 223: 2253–2267.
- [36] Roy S, Luding S, Weinhart T. A general(ized) local rheology for wet granular materials. *New Journal of Physics* 2017; 19: 043014.
- [37] Pietsch W, Rumpf H. Haftkraft, kapillardruck, flüssigkeitsvolumen und grenzwinkel einer flüssigkeitsbrücke zwischen zwei kugeln. *Chemie Ingenieur Technik* 1967; 39(15): 885–893.
- [38] Simons SJR, Seville JPK, Adams MJ. An analysis of the rupture energy of pendular liquid bridges. *Chemical Engineering Science* 1994; 49(14): 2331–2339.
- [39] Hotta K, Takeda K, Iino K. The capillary binding force of a liquid bridge. *Powder Technology* 1974; 10(4-5): 231–242.
- [40] Orr FM, Scriven LE, Rivas AP. Pendular rings between solids: meniscus properties and capillary force. *Journal of Fluid Mechanics* 1975; 67(4): 723–742.
- [41] Mazzone DN, Tardos GI, Pfeffer R. The behavior of liquid bridges between two relatively moving particles. *Powder Technology* 1987; 51(1): 71–83.
- [42] Megias-Alguacil D, Gauckler LJ. Accuracy of the toroidal approximation for the calculus of concave and convex liquid bridges between particles. *Granular Matter* 2011; 13(4): 487–492.
- [43] Israelachvili JN. *Intermolecular and Surface Forces*. Academic press . 2015.
- [44] Chau A, Rignier S, Delchambre A, Lambert P. Three-dimensional model for capillary nanobridges and capillary forces. *Modelling and Simulation in Materials Science and Engineering* 2007; 15(3): 305.
- [45] Wang J, Gallo E, François B, Gabrieli F, Lambert P. Capillary force and rupture of funicular liquid bridges between three spherical bodies. *Powder Technology* 2017; 305: 89–98.
- [46] Benzi R, Succi S, Vergassola M. The lattice Boltzmann equation: theory and applications. *Physics Reports* 1992; 222(3): 145–197.
- [47] Bhatnagar PL, Gross EP, Krook M. A model for collision processes in gases. I. Small amplitude processes in charged and neutral one-component systems. *Physical Review* 1954; 94(3): 511.
- [48] Jansen F, Harting J. From Bijels to Pickering emulsions: a lattice Boltzmann study. *Physical Review E* 2011; 83: 046707.
- [49] Davies GB, Krüger T, Coveney PV, Harting J. Detachment energies of spheroidal particles from fluid–fluid Interfaces. *Journal of Chemical Physics* 2014; 141: 154902.
- [50] Tselishchev YG, Val'tsifer VA. Influence of the type of contact between particles joined by a liquid bridge

on the capillary cohesive forces. *Colloid Journal* 2003; 65(3): 385–389.

[51] Niven RK. Force stability of pore-scale fluid bridges and ganglia in axisymmetric and non-axisymmetric configurations. *Journal of Petroleum Science and Engineering* 2006; 52(1-4): 1–18.

[52] Lees A, Edwards S. The computer study of transport processes under extreme conditions. *Journal of Physics C: Solid State Physics* 1972; 5(15): 1921.

[53] Harting J, Venturoli M, Coveney PV. Large-scale grid-enabled lattice-Boltzmann simulations of complex fluid flow in porous media and under shear. *Transactions of the Royal Society of London. Series A: Mathematical, Physical and Engineering Sciences* 2004; 362: 1703-1722.

[54] Sega M, Hantal G, Fábián B, Jedlovszky P. Pytim: A python package for the interfacial analysis of molecular simulations. 2018.

Supplementary Material

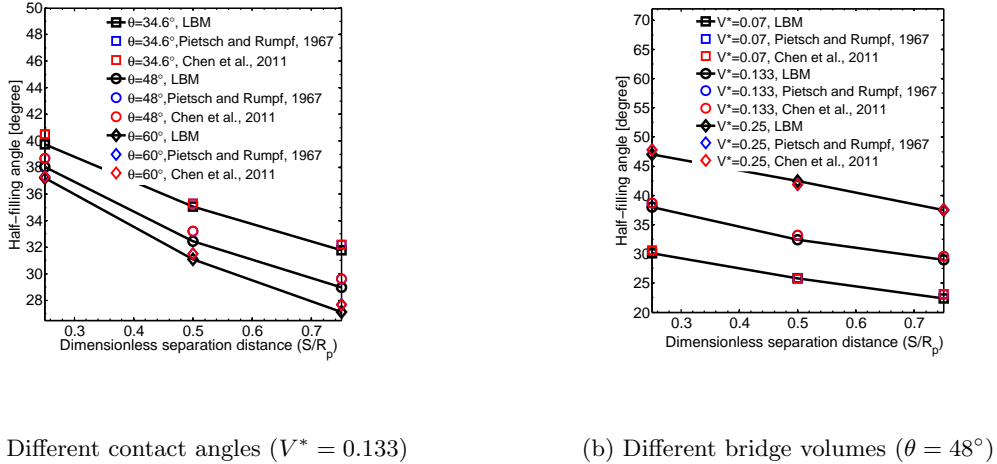


FIG. 9: Half-filling angle as a function of the separation distance under different contact angles and liquid bridge volumes between two equal spheres.

Cases	Bridge volume (V_T^*)				Error ($\frac{V_{LB}^* - V_T^*}{V_T^*}$) %			
Large V_l								
$\theta = 34.6^\circ$	$S^* = 0.286$	$S^* = 0.572$	$S^* = 0.858$	$S^* = 1.144$	$S^* = 0.286$	$S^* = 0.572$	$S^* = 0.858$	$S^* = 1.144$
	0.418	0.534	0.627	0.622	-4.4	-6.8	-7.9	2.44
$\theta = 48^\circ$	0.382	0.47	0.557	0.62	2.66	3.13	3.59	2.8
$\theta = 60^\circ$	0.366	0.485	0.583	0.657	5.11	-1.1	-2.1	-3.5
$\theta = 74^\circ$	0.373	0.503	0.531	0.603	-0.2	-5.8	6.37	4.22
Cases	Bridge volume (V_T^*)				Error ($\frac{V_{LB}^* - V_T^*}{V_T^*}$) %			
Small V_l								
$\theta = 34.6^\circ$	$S^* = 0.286$	$S^* = 0.428$	$S^* = 0.572$	$S^* = 0.858$	$S^* = 0.286$	$S^* = 0.428$	$S^* = 0.572$	$S^* = 0.858$
	0.123	0.098	0.103	0.151	8.6	5.6	4.7	3.8
$\theta = 48^\circ$	0.107	0.101	0.093	0.145	-2.6	4.5	6.9	8.0
$\theta = 60^\circ$	0.097	0.072	0.075	0.127	7.0	2.9	0.7	2.4
$\theta = 74^\circ$	0.096	0.055	0.055	0.105	-5.7	9.0	-0.9	5.5

TABLE V: Comparison of the dimensionless bridge volume ($V^* = V_l/V_p$, V_T^* from Pietsch and Rumpf, 1967, V_{LB}^* from lattice Boltzmann simulation) for equal spheres from theoretical models and Lattice Boltzmann simulations

Additional comparisons of lattice Boltzmann results with theoretical models are shown in Fig. 9 and Tables V–IX.

Figs. 9(a,b) display the half-filling angle as a function of the separation distance under different contact angles and liquid volumes. The predicted bridge filling angles from lattice Boltzmann simulations and the theoretical models from Pietsch and Rumpf [37] and Chen and coworkers [14] match well. We make comparisons between lattice Boltzmann simulations and theoretical model from Pietsch and Rumpf [37] for the prediction of the liquid bridge volume in Table V. Note that the model from Megias-Alguacil and Gauckler [7] is fully equivalent to Pietsch and Rumpf’s model for the calculation of the liquid bridge volume.

Tables VI and VII show the capillary force obtained from lattice Boltzmann simulations and the theoretical models for equal spheres. Within the range of parameters tested, the solutions by lattice Boltzmann and the theoretical models agree qualitatively, apart from bigger deviations at large contact angles (e.g., at

Cases	F^* from LB			$\frac{F_{LB}^* - F_A^*}{F_A^*}$ (% Model A)			$\frac{F_{LB}^* - F_B^*}{F_B^*}$ (% Model B)					
	Separation S^*			Separation S^*			Separation S^*					
	0.286	0.572	0.858	1.144	0.286	0.572	0.858	1.144	0.286	0.572	0.858	1.144
$\theta = 19.2^\circ$	3.03	2.87	2.7	2.52	-0.75	-3.8	-6.9	-5.2	-0.6	-3.4	-6.4	-5.3
$\theta = 34.6^\circ$	2.447	2.404	2.307	2.22	-3.0	-5.2	-6.9	-6.6	-2.9	-5.2	-6	-6.8
$\theta = 48^\circ$	1.754	1.849	2.026	2.018	-4.42	-11.5	-7.9	-9.5	-4.0	-11.1	-7.6	-9.3
$\theta = 60^\circ$	0.833	1.529	1.708	1.726	-22.1	-14.3	-14.0	-12.1	-21.2	-13	-12.5	-10.5
Cases	$\frac{F_{LB}^* - F_C^*}{F_C^*}$ (% Model C)			$\frac{F_{LB}^* - F_D^*}{F_D^*}$ (% Model D)			$\frac{F_{LB}^* - F_E^*}{F_E^*}$ (% Model E)					
	Separation S^*			Separation S^*			Separation S^*					
	0.286	0.572	0.858	1.144	0.286	0.572	0.858	1.144	0.286	0.572	0.858	1.144
$\theta = 19.2^\circ$	-2.4	2.74	6.48	9.24	-27.5	-11.3	3.6	21.8	-27.4	-24.4	-22.7	-22.2
$\theta = 34.6^\circ$	1.6	11.5	18.1	17.6	-36.5	-15.9	6.7	29.5	-23.8	-14.3	-7.7	-3.9
$\theta = 48^\circ$	6.2	19.9	38.0	29.7	-42.9	-20.2	10.4	38.9	-22.5	-6.73	13.32	23.1
$\theta = 60^\circ$	-20.6	29.5	56.9	42.6	-63.6	-37.9	11.8	57.2	-45.9	-2.9	29	57.6

TABLE VI: Comparison of the dimensionless capillary forces ($F^* = F/(\sigma R_p)$; F_A^* : F^* from model A; F_B^* : F^* from model B; F_C^* : F^* from model C; F_D^* : F^* from model D; F_E^* : F^* from model E) for equal spheres from theoretical models and Lattice Boltzmann simulations with relatively large liquid volume ($V^* = 0.4$ for $S^* = 0.286$, $V^* = 0.5$ for $S^* = 0.572$, $V^* = 0.59$ for $S^* = 0.858$, $V^* = 0.65$ for $S^* = 1.144$)

Cases	F^* from LB			$\frac{F_{LB}^* - F_A^*}{F_A^*}$ (Model A)			$\frac{F_{LB}^* - F_B^*}{F_B^*}$ (Model B)		
	Separation S^*			Separation S^*			Separation S^*		
	0.286	0.572	0.858	0.286	0.572	0.858	0.286	0.572	0.858
$\theta = 34.6^\circ$	2.527	1.852	1.64	-1.73%	-0.8%	-2.73%	-0.68%	-4.21%	-5.7%
$\theta = 48^\circ$	2	1.583	1.516	-5.5%	-3.11%	-9.06%	-5.43%	-1.66%	-7.74%
$\theta = 60^\circ$	1.324	1.216	1.242	-15.85%	-9.55%	-2.88%	-15.83%	-9.31%	-2.36%
$\theta = 74^\circ$	0.747	0.859	1.016	-13.81%	-15.32%	-2.86%	-13.41%	-15.25%	-2.69%
Cases	$\frac{F_{LB}^* - F_C^*}{F_C^*}$ (Model C)			$\frac{F_{LB}^* - F_D^*}{F_D^*}$ (Model D)			$\frac{F_{LB}^* - F_E^*}{F_E^*}$ (Model E)		
	Separation S^*			Separation S^*			Separation S^*		
	0.286	0.572	0.858	0.286	0.572	0.858	0.286	0.572	0.858
$\theta = 34.6^\circ$	-0.66%	-3.81%	-0.17%	-17.4%	25.94%	15.87%	-25.23%	-32.37%	-30.12%
$\theta = 48^\circ$	2.37%	-2.41%	2.5 %	-19.6%	38.33%	53.67%	-25.94%	-28.13%	-17.6%
$\theta = 60^\circ$	-7.86%	-8.51%	-3.91%	-20.58%	67.11%	50.3%	-38.58%	-31.48%	-11.53%
$\theta = 74^\circ$	-19.24%	-22.47 %	-9.86%	-14.76%	66.11%	60.57%	-53.93%	-40.8%	1.26%

TABLE VII: Comparison of the dimensionless capillary forces ($F^* = F/(\sigma R_p)$; F_A^* : F^* from model A; F_B^* : F^* from model B; F_C^* : F^* from model C; F_D^* : F^* from model D; F_E^* : F^* from model E) for equal spheres from theoretical models and Lattice Boltzmann simulations with relatively small liquid volume ($V^* = 0.09$ for $S^* = 0.286$, $V^* = 0.12$ for $S^* = 0.572$, $V^* = 0.15$ for $S^* = 0.858$)

$\theta = 60^\circ, 74^\circ$).

We compare the liquid bridge volume as obtained from lattice Boltzmann simulations and theoretical models by Chen and coworkers [14] and Sun and Sakai [15] in Table VIII. Table IV depicts the dimensionless capillary forces at different contact angles and separation distances. We observe good agreement between lattice Boltzmann simulations and the theoretical models with small relative errors for the predictions of the bridge volume and capillary force for different cases.

Cases	V_L^* from LB			$\frac{V_{LB}^* - V_{Chen}^*}{V_{Chen}^*}$ (Chen et al.)			$\frac{V_{LB}^* - V_S^*}{V_S^*}$ (Sun and Sakai)		
	Contact angle θ			Contact angle θ			Contact angle θ		
	34.6°	48°	60°	34.6°	48°	60°	34.6°	48°	60°
$S^* = 0.194$	0.091	0.085	0.074	2.11%	7.82%	-2.63%	4.9%	8.29%	1.14%
$S^* = 0.364$	0.098	0.089	0.081	3.56%	5.20%	8.43%	-4.20%	-13.9%	-5.2%
$S^* = 0.486$	0.112	0.108	0.099	-2.56%	4.0%	-8.29%	6.03%	-1.2%	9.37%
$S^* = 0.68$	0.128	0.127	0.118	-6.85%	-4.32%	-0.47%	10.69%	4.53%	-5.1%
$S^* = 0.85$	0.130	0.130	0.121	-9.81%	-8.64%	-9.23%	12.22%	0%	5.63%

TABLE VIII: Comparison of the dimensionless bridge volume ($V^* = V_l/V_p$; V_{Chen}^* : V^* from Chen et al.([14]); V_S^* : V^* from Sun and Sakai([15])) for unequal spheres from theoretical models and Lattice Boltzmann simulations.

Cases	F^* from LB			$\frac{F_{LB}^* - F_C^*}{F_C^*}$ (Model C)			$\frac{F_{LB}^* - F_{Chen}^*}{F_{Chen}^*}$ (Chen et al.)		
	Contact angle θ			Contact angle θ			Contact angle θ		
	34.6°	48°	60°	34.6°	48°	60°	34.6°	48°	60°
$S^* = 0.194$	2.631	1.981	1.371	-3.4%	-7.55%	-14.82%	-3.8%	-5.65%	-10.9%
$S^* = 0.364$	2.205	1.789	1.36	-6.52%	-11.35	-7.86%	-3.92%	-2.77%	-4.97%
$S^* = 0.486$	1.99	1.708	1.367	-3.06%	-7.34	-4.41%	-4.05%	-0.56%	-0.38%
$S^* = 0.68$	1.755	1.569	1.345	2.8%	-4.05	-6.11%	-1.94%	0.7%	2.1%
$S^* = 0.85$	1.494	1.404	1.202	5.38%	-2.74	3.6%	-2.86%	-1.31%	-0.623%

TABLE IX: Comparison of the dimensionless capillary forces ($F^* = F/(\sigma R_p)$; F_C^* : F^* from model C[5]; F_{Chen}^* : F^* from Chen et al.[14] and Sun and Sakai [15]) for unequal spheres from theoretical models and Lattice Boltzmann simulations.